Thermally induced permittivity enhancement in La-doped ZrO2 grown by atomic layer deposition on Ge(100)

L. Lamagna, C. Wiemer, S. Baldovino, A. Molle, M. Perego, Sylvie Schamm-Chardon, Pierre-Eugène Coulon, M. Fanciulli

Thermally induced permittivity enhancement in La-doped ZrO_2 grown by atomic layer deposition on Ge(100)

L. Lamagna, C. Wiemer, S. Baldovino, A. Molle, M. Perego, S. Schamm-Chardon, P. E. Coulon, and M. Fanciulli

Citation: Appl. Phys. Lett. **95**, 122902 (2009); doi: 10.1063/1.3227669
View online: https://doi.org/10.1063/1.3227669
View Table of Contents: http://aip.scitation.org/toc/apl/95/12
Published by the American Institute of Physics

Thermally induced permittivity enhancement in La-doped ZrO_2 grown by atomic layer deposition on Ge(100)

L. Lamagna,[1,a] C. Wiemer,[1] S. Baldovino,[1] A. Molle,[1] M. Perego,[1] S. Schamm-Chardon,[2] P. E. Coulon,[2] and M. Fanciulli[1,3]
[1]*Laboratorio Nazionale MDM, CNR-INFM, Via C. Olivetti 2, 20041 Agrate Brianza (MI), Italy*
[2]*CEMES-CNRS and Université de Toulouse, nMat group, BP 94347, 31055 Toulouse cedex 4, France*
[3]*Dipartimento di Scienza dei Materiali, Università degli Studi di Milano-Bicocca, 20126 Milano, Italy*

(Received 6 July 2009; accepted 19 August 2009; published online 23 September 2009)

La-doped ZrO_2 thin films grown by O_3-based atomic layer deposition directly on Ge(100) exhibit a dielectric constant of 29. Upon annealing in N_2 at 400 °C, a high κ value >40 is extracted for film thickness below 15 nm. Compositional depth profiling allows to correlate this observation with a remarkable Ge interdiffusion from the substrate which is consistent with the stabilization of the tetragonal ZrO_2 phase. Ge interaction with the oxide stack and the formation of a germanate-like interfacial region, which acts as an electrical passivation for the Ge surface, are also investigated.
 [doi:10.1063/1.3227669]

As alternative to Si in high-speed logic devices, Ge is widely considered due to its higher carrier mobilities.[1,2] Coupling Ge channel with high dielectric constant (κ) material is a promising strategy for ultrascaled logic devices. Among high-κ oxides, ZrO_2 has been proved to be a promising insulator. Numerous results were presented for ZrO_2/Ge stacks grown by sputtering,[3,4] atomic layer deposition (ALD)[5–7] and molecular beam deposition (MBD).[8] Interface engineering still remains an open issue as the Ge/oxide interface exhibits an unacceptably large density of interface traps (D_{it}), which can be related to Ge dangling bond interface defects.[9,10] A broad range of solutions was considered, e.g. Ge controlled oxidation[6,11] and deposition of passivating interfacial layer (IL).[12] Recently, a study on ZrO_2/GeO_2 stacks prepared by atomic oxygen-assisted MBD (Ref. 8) correlates a very high κ value (~44) with the promotion of tetragonal ZrO_2. Such a large κ is there associated with Ge incorporation into the ZrO_2 due to thermal decomposition of the GeO_2 IL. In our work, we focus on O_3-based ALD of La-doped ZrO_2 (La–ZrO_2) on Ge(100) therein targeting the growth of a high-κ material through a direct deposition approach without IL. As-grown and annealed La–ZrO_2 films were characterized by means of (i) high resolution transmission electron microscopy (HRTEM) coupled to electron energy-loss spectroscopy (EELS), and selected area electron diffraction (SAED), (ii) x-ray photoemission spectroscopy (XPS), (iii) time of flight secondary ion mass spectroscopy (ToF SIMS), and (iv) capacitance-voltage (C-V) measurements. La–ZrO_2 films were grown at 300 °C in a Savannah 200 (Cambridge Nanotech Inc.) ALD reactor on n-type Ge(100). Native GeO_2 was removed in a diluted HF solution (1:25). La incorporation in ZrO_2 (~5% mean value) should enhance the κ value through doping induced effect.[13,14] La can also favor the interfacial La–O–Ge bonds, thus reducing Ge suboxides and electronic traps.[15,16] In this respect, O_3 oxidation was demonstrated to opportunely passivate Ge interface.[17,18] This motivates our choice to start the ALD with a La_2O_3 step and to choose O_3 (~200 g/Nm^3) as oxidizer. Precursors were $(^i PrCp)_3La$ and $(MeCp)_2ZrMe(OMe)$ (SAFC Hitech). The ALD cycle number varied from 8 to 80, stack thickness was estimated using spectroscopic ellipsometry and x-ray reflectivity (XRR) in the 3–30 nm range. La doping was tuned by the ALD La/Zr ratio. Postgrowth rapid thermal annealing (RTA) was performed for 60 s in N_2 at 400 °C.

Room temperature C-V measurements were performed on metal insulator semiconductor capacitors; capacitance equivalent oxide thickness (CET) was determined from the accumulation capacitance (C_{acc}) at 100 kHz. Figure 1(a) illustrates multifrequency C-V curves obtained for an as-grown La–ZrO_2 film. Only weak frequency dispersion is observed both in accumulation and depletion, indicating a relatively low D_{it} ($\sim 8 \pm 1 \times 10^{11}$ eV^{-1} cm^{-2} evaluated with the Hill–Coleman method[19] at 500 kHz). For the as-grown stack a $\kappa = 18 \pm 1$ can be calculated from the C_{acc} by applying a single-layer capacitor model. Figure 1(b) displays multifrequency C-V curves obtained after annealing. A clockwise hysteresis of 550 (as-grown) and 850 (annealed) mV is measured. C-V curves appear more stretched and only a moderate increase of the D_{it} up to $\sim 2 \pm 1 \times 10^{12}$ eV^{-1} cm^{-2} is observed. After annealing, the C_{acc} is noticeably higher than the one related to the as-grown state thus suggesting a significant impact of the RTA on the dielectric properties. Applying a capacitor model a $\kappa = 21 \pm 1$ for the annealed stack is calculated.

A structural and chemical investigation of the Ge(100)/La–ZrO_2 interface and within the film was per-

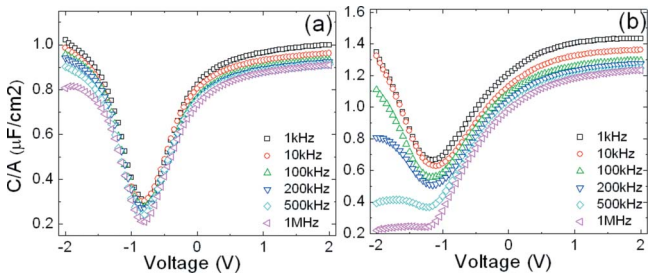

FIG. 1. (Color online) (a) C-V characteristics for Al-gate (0.85×10^{-5} cm^2) MIS capacitors fabricated from a 14.5 nm thick as-grown sample and (b) from a 14.4 nm thick annealed sample.

[a]Author to whom correspondence should be addressed. Electronic mail: luca.lamagna@mdm.infm.it.

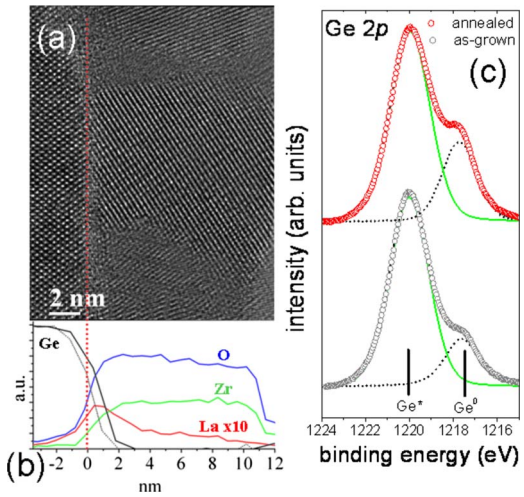

FIG. 2. (Color online) (a) HRTEM cross section of annealed La–ZrO_2 film (14 nm). (b) STEM-EELS profiles for the as-grown (dotted line) and annealed (plain line) case. For clarity, only the Ge profile is shown for the as-grown case since Zr, O, and La profiles remain almost stable upon annealing. (c) Ge 2*p* XPS lines of the as-grown and annealed 3 nm thick La–ZrO_2 film with $\psi=90°$.

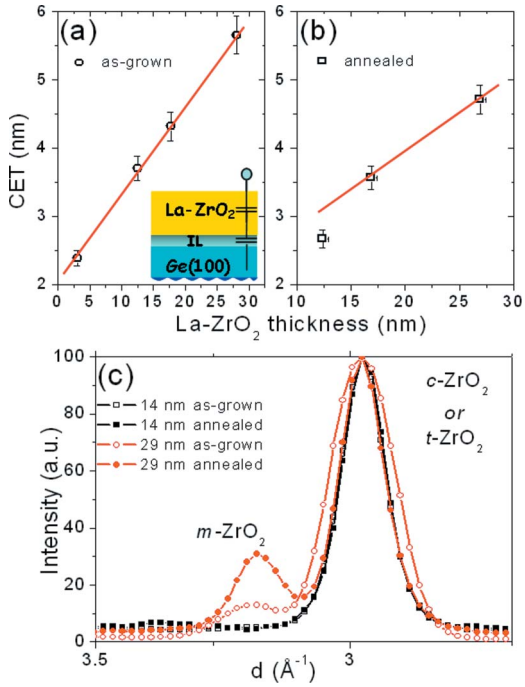

FIG. 3. (Color online) (a) CET vs La–ZrO_2 thickness plot for as-grown samples. MIS devices received no postmetallization annealing. Inset shows the two capacitors model (La–ZrO_2/IL/Ge). (b) CET vs La–ZrO_2 thickness plot for annealed samples. (c) SAED intensity profiles acquired on 29 and 14 nm thick as-grown and annealed samples.

formed with HRTEM and EELS on the 14 nm thick sample before and after RTA (for details on TEM see Ref. 20). As-grown films are crystalline for all the analyzed thicknesses, as also proved by x-ray diffraction (not shown), with a cubic (*c*-) and/or tetragonal (*t*-) phase of ZrO_2 which cannot be univocally assigned [Fig. 3(c)]. Differently from $La_{0.25}Zr_{0.75}O_{2-\delta}$/Si (Ref. 21) the very low La content does not promote the amorphization of the ZrO_2 matrix. A direct contact between the La–ZrO_2 crystals and Ge(100) is observed also after RTA [Fig. 2(a)]. Consequently, there is no IL from the structural viewpoint. A chemical interfacial region is revealed as evidenced on the La, Zr, O, and Ge elemental STEM-EELS profiles as a function of the distance from the substrate by scanning a 1 nm probe diameter up to the film surface [Fig. 2(b)]. The Zr and O profiles increase just after the substrate and beyond few nm become constant with a Zr/O ratio ~0.5. The La profile has a peak just above the interface, the intensity at the maximum being La/Zr ~0.1 and then continuously decreases. The La, Zr, and O profiles are very similar in the as-grown and annealed state. First, Ge is present above the interface with a non-negligible content in the region of the La peak. After RTA, Ge profile has a similar shape but spreads over a larger distance from the substrate. STEM-EELS profiles reveal a La and Ge rich region near the interface different from the following region of nearly constant composition. Hence, the as-grown and annealed films can be described by a two layers structure from the chemical viewpoint. From the Ge profiles, we can infer that a 2 nm thick IL (as-grown) and a nearly 2.5 nm thick IL (after RTA) is present [dots and lines respectively, Fig. 2(b)]. The chemical bonding at the interface were probed by XPS analyses of the Ge 2*p* line performed on 3 nm thick as-grown and annealed samples [Fig. 2(c)] in normal photoemission geometry through a standard Mg $K\alpha$ (1253.6 eV) radiation source. Both the Ge 2*p* lines can be deconvoluted in two different contributions from the elemental Ge bonding of the substrate (Ge^0) and Ge–O like bonding (Ge^*). The mutual shift between the two components is 2.3 eV, which deviates from the expected shift due to GeO_2 and suggests the formation of a germanate-like region before and after RTA.[22] The increased intensity of the Ge^0 contribution after annealing reflects a thermally induced reduction of the stack thickness. XRR analysis (same samples, not shown) also revealed a reduction of total thickness and a corresponding 10% electronic density increase upon RTA related to a densification of the whole layer. The formation of a germanate IL, associated to the use of O_3, might help to keep the D_{it} value relatively low.

Electrical results are discussed based on the previous analysis. Figure 3(a) shows a linear dependence of the CET versus La–ZrO_2 physical thickness plot, leading to $\kappa=29\pm1$ for the as-grown films. This κ value resembles the one expected for *c*- and is higher than the one of monoclinic (*m*-)ZrO_2 (~20), thermodynamically stable on Si(100).[23,24] An active role in determining the κ of as-grown films might be played by the large ionic radius ($i_{rad}\sim1.23$ Å) of La atoms, inserted into the ZrO_2 lattice, softening the ZrO_2 IR-active modes.[21,25] The intercept of the linear fit to the CET data confirms the presence of an IL between La–ZrO_2 and Ge(100) and clarifies the higher κ values of La–ZrO_2 compared to the one of the stack. Given a 2 nm thick IL, as revealed by STEM-EELS, a low IL κ ($\kappa_{IL}=4$) is calculated. The use of this IL in a two capacitors model [inset of Fig. 3(a)] results in a $\kappa=28\pm1$ for the as-grown La–ZrO_2. After RTA, CET versus La–ZrO_2 thickness plot [Fig. 3(b)] cannot be interpolated by a linear fit. This finding can be clarified by structural and chemical modifications within the films depending on the thickness as illustrated in Figs. 3(c) and 4. Figure 3(c) shows the SAED analyses performed on the thickest (29 nm) and the thinnest (14 nm) stacks before and after RTA. The *m*-ZrO_2 phase is revealed in the thick (19 and 29 nm) as-grown samples and such *m*-fraction increases upon annealing. Differently, 14 nm thick film is free of *m*-ZrO_2. A linear estimation of the κ, for the two thickest

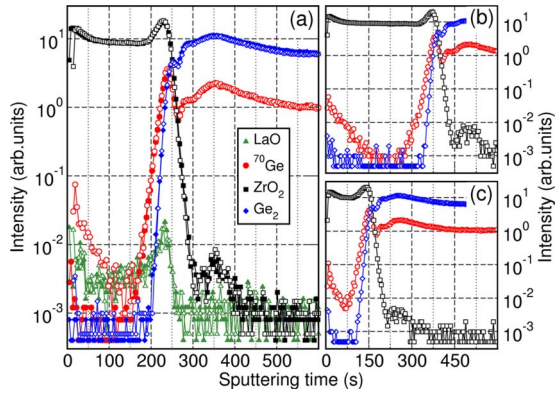

FIG. 4. (Color online) (a) ToF SIMS depth profile for 19 nm thick, as-grown (closed symbols) and annealed (open symbols), La–ZrO_2 film. ToF SIMS depth profiles for 29 (b) and 14 (c) nm thick annealed La–ZrO_2 films.

annealed stacks results in a $\kappa=34\pm1$ [Fig. 3(b)]; given a 2.5 nm thick IL (from STEM-EELS) a $\kappa_{IL}=6.2$ is calculated from the fit intercept. This value is in agreement with the presence of a comparatively denser germanate compound at the interface or with κ values proposed for germanates.[22,26] The use of these IL parameters in a two capacitors model provides a $\kappa=32\pm1$ for the thick annealed films (19 and 29 nm) whereas for the thinner annealed La–ZrO_2 the κ is remarkably increased up to $\sim42\pm1$. Such result confirms that the 14 nm thick film is structurally different. To assess the elemental composition after RTA, ToF SIMS depth profiles were acquired in negative polarity on an ION-TOF IV instrument using Cs^+ ions at 1 keV for sputtering and Ga^+ ions at 25 keV for analysis. Upon RTA, LaO and ZrO_2 signals are not modified [Fig. 4(a)] whereas Ge diffusion throughout the oxide is evidenced by the ^{70}Ge signal. The level of Ge should be low because it was not observed by STEM-EELS with a sensitivity limit for Ge around 3–5%. Ge can be inferred to diffuse up to the top of the La–ZrO_2 layer directly from the substrate; its diffusion strongly depends on film thickness as shown by the different ^{70}Ge profiles [Figs. 4(a)–4(c)]. Actually, the presence of a Ge-poor region is more pronounced in thicker films and therefore these dissimilar chemical profiles might be associated with variable crystalline mixtures in the films. Hence, Ge diffusion is expected to cause the absence of *m*-ZrO_2 phase in the 14 nm sample and thus the increase of La–ZrO_2 κ after RTA. Interdiffused Ge might play a role in stabilizing the *t*-ZrO_2 phase, as proposed in Refs. 8 and 13, since the κ of the thicker samples also slightly increases after RTA despite the development of the *m*-phase. Indeed, pronounced electrical differences are accompanied in the thinnest annealed sample by a remarkable Ge diffusion. It should be noted that, when ZrO_2 was deposited on a La_2O_3 IL, only a $\kappa\sim32$ for ZrO_2 was measured.[22] Differently from Refs. 8, 22, and 27, La–ZrO_2 was directly deposited on Ge(100) without IL. The observed κ enhancement is consistent with the prediction by Fischer *et al.*[13] that, upon introduction of Ge substitutional atoms, *t*-ZrO_2 can become energetically more favorable than *m*- or *c*-phases. Ge atoms, with a small i_{rad} (~0.53 Å), are readily incorporated in the thin La–ZrO_2 layer therein promoting the stabilization of *t*-ZrO_2. Although the revealed Ge concentration in La–ZrO_2 is lower than the one theoretically predicted, this amount is enough to stabilize *t*-ZrO_2.[28]

In summary, we showed that the combination of a direct O_3-based ALD of La–ZrO_2 and RTA can lead to a $\kappa>40$. It is proved that Ge atoms are supplied by the substrate and penetrate into the oxide upon annealing. The observed large κ value after RTA is consistent with Ge-induced stabilization of the *t*-ZrO_2 phase in thin film. Ge diffusion occurs without affecting the interfacial details qualified by a germanate-like region and an acceptably low D_{it} value.

We acknowledge G. Seguini, A. Lamperti and G. Congedo (MDM). Work was supported by the European FP6-Program "REALISE" (Grant No. IST-NMP016172).

[1] B. H. Lee, J. Oh, H. H. Tseng, R. Jammy, and H. Huff, Mater. Today **9**, 32 (2006).
[2] Y. Kamata, Mater. Today **11**, 30 (2008).
[3] Y. Kamata, Y. Kamimuta, T. Ino, R. Iijima, M. Koyama, and A. Nishiyama, Jpn. J. Appl. Phys., Part 1 **45**, 5651 (2006).
[4] Y. Kamata, Y. Kamimuta, T. Ino, and A. Nishiyama, Jpn. J. Appl. Phys., Part 1 **44**, 2323 (2005).
[5] J. Oh, P. Majhi, C. Y. Kang, J.-W. Yang, H.-H. Tseng, and R. Jammy, Appl. Phys. Lett. **90**, 202102 (2007).
[6] A. Delabie, F. Bellenger, M. Houssa, T. Conard, S. Van Elshocht, M. Caymax, M. Heyns, and M. Meuris, Appl. Phys. Lett. **91**, 082904 (2007).
[7] H. Kim, C. O. Chui, K. C. Saraswat, and P. C. McIntyre, Appl. Phys. Lett. **83**, 2647 (2003).
[8] P. Tsipas, S. N. Volkos, A. Sotiropoulos, S. F. Galata, G. Mavrou, D. Tsoutsou, Y. Panayiotatos, A. Dimoulas, C. Marchiori, and J. Fompeyrine, Appl. Phys. Lett. **93**, 082904 (2008).
[9] M. Caymax, M. Houssa, G. Pourtois, F. Bellenger, K. Martens, A. Delabie, and S. Van Elshocht, Appl. Surf. Sci. **254**, 6094 (2008).
[10] S. Baldovino, A. Molle, and M. Fanciulli, Appl. Phys. Lett. **93**, 242105 (2008).
[11] A. Molle, Md. N. K. Bhuiyan, G. Tallarida, and M. Fanciulli, Appl. Phys. Lett. **89**, 083504 (2006).
[12] H. J. Na, J. C. Lee, D. Heh, P. Sivasubramani, P. D. Kirsch, J. W. Oh, P. Majhi, S. Rivillon, Y. J. Chabal, B. H. Lee, and R. Choi, Appl. Phys. Lett. **93**, 192115 (2008).
[13] D. Fischer and A. Kersch, Appl. Phys. Lett. **92**, 012908 (2008).
[14] C. K. Lee, E. Cho, H. S. Lee, C. S. Hwang, and S. Han, Phys. Rev. B **78**, 012102 (2008).
[15] G. Mavrou, S. Galata, P. Tsipas, A. Sotiropoulos, Y. Panayiotatos, A. Dimoulas, E. K. Evangelou, J. W. Seo, and C. Dieker, J. Appl. Phys. **103**, 014506 (2008).
[16] M. Houssa, G. Pourtois, M. Caymax, M. Meuris, and M. M. Heyns, Appl. Phys. Lett. **92**, 242101 (2008).
[17] D. Kuzum, T. Krishnamohan, A. J. Pethe, A. K. Okyay, Y. Oshima, Y. Sun, J. P. McVittie, P. A. Pianetta, P. C. McIntyre, and K. C. Saraswat, IEEE Electron Device Lett. **29**, 328 (2008).
[18] S. Spiga, C. Wiemer, G. Tallarida, G. Scarel, S. Ferrari, G. Seguini, and M. Fanciulli, Appl. Phys. Lett. **87**, 112904 (2005).
[19] W. A. Hill and C. C. Coleman, Solid-State Electron. **23**, 987 (1980).
[20] S. Schamm, P. E. Coulon, S. Miao, S. N. Volkos, L. H. Lu, L. Lamagna, C. Wiemer, D. Tsoutsou, G. Scarel, and M. Fanciulli, J. Electrochem. Soc. **156**, H1 (2009).
[21] D. Tsoutsou, L. Lamagna, S. N. Volkos, A. Molle, S. Baldovino, M. Fanciulli, S. Schamm, and P. E. Coulon, Appl. Phys. Lett. **94**, 053504 (2009).
[22] G. Mavrou, P. Tsipas, A. Sotiropoulos, S. F. Galata, Y. Panayiotatos, A. Dimoulas, C. Marchiori, and J. Fompeyrine, Appl. Phys. Lett. **93**, 212904 (2008).
[23] X. Zhao and D. Vanderbilt, Phys. Rev. B **65**, 075105 (2002).
[24] O. Ohtaka, D. Andrault, P. Bouvier, E. Schultz, and M. Mezouar, J. Appl. Crystallogr. **38**, 727 (2005).
[25] S. A. Shevlin, A. Curioni, and W. Andreoni, Phys. Rev. Lett. **94**, 146401 (2005).
[26] J. Song, K. Kakushima, P. Ahmet, K. Tsutsui, N. Sugii, T. Hattori, and H. Iwai, Microelectron. Eng. **84**, 2336 (2007).
[27] D. Tsoutsou, G. Apostolopoulos, S. Galata, P. Tsipas, A. Sotiropoulos, G. Mavrou, Y. Panayiotatos, and A. Dimoulas, Microelectron. Eng. **86**, 1626 (2009).
[28] D. Fischer and A. Kersch, J. Appl. Phys. **104**, 084104 (2008).